Calculation of gas heating in a dc sputter magnetron

I. Kolev[a] and A. Bogaerts
Research Group PLASMANT, Department of Chemistry, University of Antwerp, Universiteitsplein 1, 2610 Antwerp, Belgium

(Received 7 March 2008; accepted 23 June 2008; published online 6 November 2008)

The effect of gas heating in laboratory sputter magnetrons is investigated by means of numerical modeling. The model is two-dimensional in the coordinate space and three-dimensional in the velocity space based on the particle-in-cell–Monte Carlo collisions technique. It is expanded in a way that allows the inclusion of the neutral plasma particles (fast gas atoms and sputtered atoms), which makes it possible to calculate the gas temperature and its influence on the discharge behavior in a completely self-consistent way. The results of the model are compared to experimental measurements and to other existing simulation results. The results show that gas heating is pressure dependent (rising with the increase in the gas pressure) and should be taken into consideration at pressures above 10 mTorr. © *2008 American Institute of Physics*. [DOI: 10.1063/1.2970166]

I. INTRODUCTION

The volume in front of the cathode in a sputter magnetron has to be viewed as a highly dynamic region. Except for the main ingredients of the plasma, i.e., charged particles and equilibrium gas atoms, there exist additional energetic species such as reflected, neutralized gas ions, gas atoms born in charge exchange collisions, and nonthermal sputtered atoms. All of them can participate in momentum transfer collisions with the cold, background gas atoms. These collisions are expected to be highly effective, due to the similar masses of the colliding partners. In this way, significant energy and momentum can be deposited from the energetic species to the volume of the background gas, giving rise to a temperature increase in the gas and, consequently, creating a density inhomogeneity through the ideal gas law. These density fluctuations can influence the whole discharge because of the dependency of the cross sections of all major collisions on the gas density. Most of the energetic species are created either at the cathode (sputtered atoms, reflected, and neutralized ions) or in the sheath (atoms generated by charge exchange collisions). This brings a large amount of directionality to the energy and momentum transfer. In addition to that, the distribution of the bombarding fluxes at the cathode is nonuniform, as is also demonstrated experimentally by race-track profiles. Thus, there can be expected a large degree of nonuniformity in the dynamics of the gas and the sputtered atoms. This particularity of the magnetron operation has been referred to as sputtering wind, a name given by Hoffman.[1]

The gas heating and the corresponding reduction in the gas density at a given pressure, also known as gas rarefaction, is a function of three factors. The first one is the available energy in the discharge. It depends on the power introduced in the discharge by the external power supply.

The second factor is the ability of the background gas to absorb the available energy. The absorption is via binary collisions and their rate is proportional to the gas density. Therefore, the two main operating parameters, upon which the gas heating depends on, are the applied power and the gas pressure. This claim has been experimentally confirmed by Rossnagel,[2] who reports a maximum gas reduction of 85% at 3 kW input power and by the simulations reported in Ref. 3.

Besides the operating conditions, the gas heating is also a function of the type of atoms into consideration. This is the third factor and it plays a role because the sputtering yield is material sensitive and so is the reflection coefficient. The latter determines what fraction of the energetic gas atoms will be reflected back into the discharge after hitting the cathode or the vessel walls. This is important because the mean free path of the gas atoms at typical pressures of a magnetron discharge (i.e., several pascals) is about two centimeters, and they need several collisions before being thermalized.[4]

The possible gas density fluctuations and corresponding energy exchange reactions are important for the energy flux at the substrate and therefore for the film growth quality. Despite that, the papers devoted to give a quantitative estimate of the extent and the effect of gas heating in magnetrons are limited. They include the combination of an experimental and global energy balance modeling,[2] a non-self-consistent Monte Carlo (MC) simulation,[5] a theoretical approach,[6] and a non-self-consistent, fluid heat flow calculation.[3] Only the last work is not one dimensional. The main uncertainties in these papers are the estimated (assumed) number of collisions, both in the volume and at the cathode, as well as their spatial distribution. This weakness is a direct result of the lack of a model that treats simultaneously and self-consistently the whole magnetron plasma. Such model should give the exact, spatially resolved source terms for the heat transfer based on the real energy exchange processes. Three such models that fulfill this requirement have been reported for other types of discharges. The first one is for sputtering in a nonmagnetized dc glow discharge.[7] It is one-dimensional in the coordinate space and three-dimensional in the velocity space (1d3v) particle-in-cell–MC collisions (PIC/MCC) simulation with an incorporated heat module.

The other two are for analytical dc glow discharges in

[a]Electronic mail: ivan.kolev@ua.ac.be.

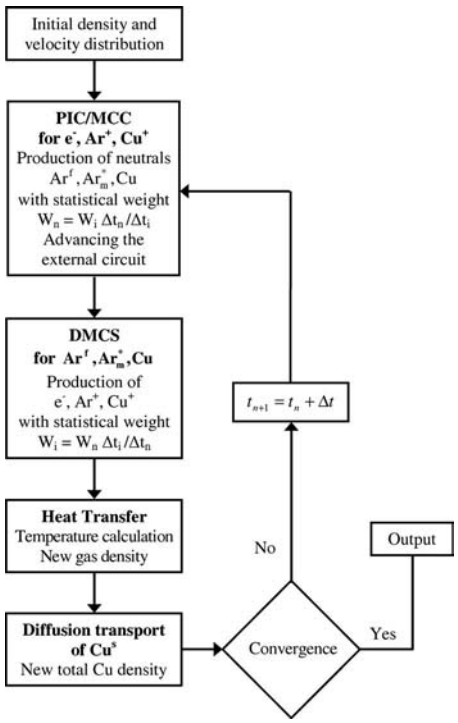

FIG. 1. Flowchart of the simulation procedure for calculation of gas heating. The abbreviation DMCS stands for "direct Monte Carlo simulation."

argon.[8,9] They are, however, not applicable to magnetrons because they are hybrid MC-fluid models, whereas a full kinetic description is necessary to cope with the low pressure and strong magnetic field typical for sputtering magnetrons.[10]

In the present work, a self-consistent PIC/MCC model, suitable for axisymmetric dc sputter magnetrons (cylindrical, 2d3v) and capable of calculating the gas heating and its effects, is applied to a commercially available magnetron in order to investigate gas heating in laboratory sputter magnetrons. The investigation is in the gas pressure range of 1–100 mTorr for a copper cathode in argon.

II. DESCRIPTION OF THE MODEL

A. Numerical procedure

The present model is represented in Fig. 1. Most of its features have been discussed in Ref. 11. Here, a summary of the main aspects will be given, together with details directly related to the calculation of gas heating.

The PIC/MCC part of the model for the charged particles (see Fig. 1), including an external circuit, has been explained in detail in our previous work.[12] There, all computational details, such as stability criteria, grid size, and superparticle size, can be found. The external circuit secures that the simulated magnetron is operated in the desired regime of its voltage-current characteristic. In this simulation, a simple circuit, consisting of a constant voltage source and a ballast resistor in series with the discharge, is employed. The coupling between the circuit and the discharge is maintained via satisfying the charge conservation at the cathode. In this way, the cathode potential results as a balance of the applied external voltage and the charge deposited on the cathode from the discharge. The details about the inclusion of the circuit are given originally in Ref. 13. The full procedure, together with a thorough discussion about the importance of the external circuit, can also be found in Ref. 14.

The whole simulation needs to be run until convergence is obtained. This numerical convergence must be correlated with the achievement of steady state by the real physical system that is the subject of the simulation. The time necessary for the physical system to reach a steady state is determined by the slowest processes in the system. When the heating of the gas is taken into consideration, the characteristic time τ_H for thermal equilibrium (i.e., bringing the heat conduction to a steady state) is the longest—$\tau_H \sim 10^{-2}$ s. This estimate is based on the relation[15]

$$\tau_H = \frac{L}{V_H} = \frac{c_p \rho L^2}{k}.$$

Here, $L(\simeq 0.1$ m) (Ref. 7) is the characteristic diffusion length, V_H is the characteristic speed of heat transfer, c_p is the specific heat per unit mass at constant pressure, ρ $(=7.97\times 10^{-5}$ kg/m$^3)$ (Ref. 16) is the argon mass density, and k $(=0.018$ W m^{-1} K$^{-1})$ (Ref. 16) is the thermal conductivity of argon.

At the same time, the characteristic time for bringing the electrons and the ions to a steady state does not exceed 10^{-5} s.[17] All other important processes such as the relaxation time for thermalization of the energetic neutrals and pressure equalization are situated in between these two limits.[7,17] Because of this big difference in the characteristic times of the electrons, ions, fast neutrals, and thermal conduction, some modifications in the general PIC/MCC algorithm are necessary to cope with this disparity when neutrals and heat transfer have to be added to the model. Not doing so would result in a huge amount of computational time. This is so because of the general restriction for the time step Δt.[18]

$$\omega_{\mathrm{ch}} \Delta t \approx 0.2, \tag{1}$$

where ω_{ch} is the highest characteristic frequency in the magnetron. Thus, the fastest processes require a small enough time step, while the slowest processes demand the whole simulation to be run long enough; i.e., the number of the time steps (computational cycles) increases unacceptably. The procedure used here[7] is to advance the different sorts of particles with different time steps. The hierarchy being $\Delta t_e \ll \Delta t_i \ll \Delta t_n$ [e (electron), i (ion), and n (neutral)]. This difference in the time steps is accounted for by the weight W of the produced energetic, charge exchange neutrals, and sputtered atoms, i.e.,

$$W_n = W_s = W_i \frac{\Delta t_n}{\Delta t_i}, \tag{2}$$

where s refers to the sputtered atoms. Moreover, electrons are subcycled inside the ion time step and have $W_e = W_i$. In this way, it is assured that the production and loss rates of the real plasma particles are correctly represented; i.e., the global mass conservation is obeyed.

The procedure separates the particles into two groups: fast and slow. The upper size of the superparticles from each

group can be controlled independently of the corresponding value of the other group. When the upper limit is reached, only the members of the corresponding group are reduced twice and their weight is doubled. The weight and number of the superparticles from the other group are not changed. However, a change in the time step is needed in order to maintain Eq. (2) as valid. Because Δt_i is coherent with the stability criterion of the PIC method [see Eq. (1) above], the time step that always changes is $\Delta t_n (=\Delta t_s)$.

The heat transfer can occur by conduction or/and convection. Whichever of the two mechanisms is dominant, if any, it is commonly determined by the Peclet number

$$\mathrm{Pe} = \frac{V}{V_H} = \frac{c_p \rho V L}{k},$$

where V is the flow velocity and the other symbols have been explained above. A calculation of the flow velocity in conditions similar to those in the present work reads $V \approx 1$ m/s.[19] Based on that, the Peclet number is $\mathrm{Pe} \approx 0.2$. Thus, it can be accepted with sufficient accuracy that for the given operating conditions the heat transfer is governed by conduction. Deviations from this regime can be expected if the flow of the feeding gas is strong. This, however, is out of the scope of the present work.

The overall computational cycle consists of one ion time step. At the end of it, the power P, transferred to and from the feeding gas, is accumulated,

$$P = \frac{m_g W_n}{V_{\mathrm{cell}} \Delta t_n} \left[\sum_l \frac{v_l'^2 - v_l^2}{2} - \sum_l \frac{v_l^2}{2} + \sum_l \frac{v_l'^2}{2} \right], \tag{3}$$

where $\boldsymbol{v}_l'$ is the post and the precollision velocity of the lth gas atom, m_g is the gas mass, and V_{cell} is the volume of the computational grid cell. The first sum is the contribution from all collisions between the feeding gas atoms from one side and the ions, fast atoms, metastable atoms, and sputtered atoms from the other side. Only collisions, in which the post-collision energy of the gas atoms is less than some threshold, are counted. This threshold is chosen to be[7]

$$E_{\mathrm{th}} = 9 \times \tfrac{3}{2} k_b T_g, \tag{4}$$

where k_b is the Boltzmann constant. The other collisions result in creation of fast gas atoms, which are incorporated by the second sum. The third sum is the contribution of the thermalized fast gas atoms. This calculated power is used as a source term in the heat conduction equation, which in cylindrical (r,z) coordinates is

$$\frac{\partial^2 T_g}{\partial z^2} + \frac{1}{r}\frac{\partial}{\partial}\left(r \frac{\partial T_g}{\partial r} \right) = -\frac{P}{k}, \tag{5}$$

and is solved once per 10^{-8} s (actually, after each number of time steps divisible exactly by 100 and whose sum is greater than or equal to 10^{-8} s) to calculate the gas temperature T_g. In the above equation, k is the thermal conductivity of the gas. Equation (5) is solved with a boundary condition $T = 300$ K at all walls including the cathode. While at the surrounding walls such condition is natural, at the cathode the temperature can be higher due to the bombardment of the energetic particles. Therefore, a strict boundary condition at the cathode should be obtained by solving an equation for the thermal conductivity of the cathode. Our choice to use a fixed temperature is aimed toward simplification of the calculations and based on the following. Normally, cathodes are cooled by water, exactly to prevent them from heating. Also, the applied power in the present study is relatively moderate.

It should be mentioned that T_g is a dynamic quantity dependent on the coordinates. Consequently, the threshold energy given by Eq. (4) is also dynamic (changes with time) and is a function of the coordinates.

The sputtered atoms are followed as particles until thermalized. Once that happens, they cannot anymore contribute to gas heating directly; collisions between fast argon atoms and sputtered atoms are disregarded in the model because of the statistical insignificance of the process. The overall copper density, however, is important for the application of magnetron sputter deposition of thin films. Therefore, a compromise between accuracy of the algorithm and its computational efficiency is to treat the thermalized copper atoms as fluid. Thus, the overall copper density is a sum of the density of the fast copper atoms and the slow copper atoms. The density of the slow (thermalized) copper atoms $n_{\mathrm{Cu}}^{\mathrm{sl}}$ can be obtained by solving the diffusion equation, which in (r,z) cylindrical coordinates reads

$$D_{\mathrm{Cu}} \Delta n_{\mathrm{Cu}}^{\mathrm{sl}}(r,z) = r_{\mathrm{loss}}(r,z) - r_{\mathrm{prod}}(r,z), \tag{6}$$

where D_{Cu} is the diffusion coefficient of copper atoms in argon, r_{loss} is the rate of loss of the slow copper atoms, and r_{prod} is their production rate. The diffusion coefficient is obtained from the value $D_{\mathrm{Cu}} = 1.44 \times 10^{-2}$ cm^2 s^{-1},[20] which is based on the rigid-sphere collision model and refers to a pressure of 1 Torr and a temperature at 300 K in argon. The recalculation of the diffusion coefficient for the simulation conditions (pressure p and gas temperature T_g) is done as

$$D_{\mathrm{Cu}}(p) = D_{\mathrm{Cu}}(p = 1 \ \mathrm{Torr}) \frac{1000}{p \ (\mathrm{mTorr})} \frac{T_g \ (\mathrm{K})}{300}.$$

The loss rate of the copper atoms $r_{\mathrm{loss}}(r,z)$ is equal to the rate of ionization of the copper atoms caused by all ionization mechanisms: electron impact, Penning ionization, and asymmetric charge transfer. The production rate of the copper atoms $r_{\mathrm{prod}}(r,z)$ is equal to the rate of thermalization of the sputtered atoms.

Equation (6), as well as Eq. (5), is mathematically the same as the Poisson equation for the potential. Therefore, the same numerical technique, cyclic reduction,[21] is used for their solution (see Ref. 11 for more details). The boundary conditions of Eq. (6) are $\nabla^2 n_{\mathrm{Cu}}^{\mathrm{sl}}|_{\mathrm{wall}} = 0$ and $\nabla_r [n_{\mathrm{Cu}}^{\mathrm{sl}}(0,z)] = 0$. The latter represents simply the cylindrical symmetry of the system.

B. Included species in the model and their collision processes

The model includes the following plasma particles: electrons, singly charged argon (Ar^+) and copper (Cu^+) ions, energetic (fast) argon atoms (Ar^f), metastable argon atoms (Ar_m^*), and copper atoms (Cu). The metastables are included for their role in the production of copper ions by Penning

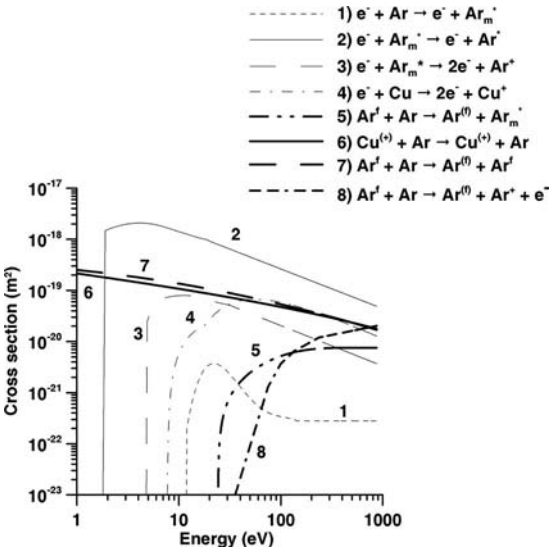

FIG. 2. Cross sections of some of the important collisions included in the model. The thin-line collisions involve electrons: (1) electron-impact excitation of the argon atom to the metastable level (Ref. 27), (2) electron-impact transition from the metastable to the irradiative excited state of the argon atom (Ref. 28), (3) electron-impact ionization of the metastable argon atom (Ref. 29), and (4) electron-impact ionization of the copper atom (Ref. 30). The bold-line collisions are between heavy particles: (5) argon atom-induced excitation to the metastable level of the argon atom (Ref. 31), (6) elastic scattering of copper atoms and ions from argon atoms (Ref. 32), (7) elastic scattering of fast argon atoms and ion with argon background gas atoms (Ref. 33), and (8) argon atom-impact ionization of the argon atom (Ref. 34).

ionization. The collisions between the electrons and argon ions from one side and the background argon atoms from the other side have been discussed in Ref. 12.

Although Penning ionization has been known for a long time, there is a lack of cross section data based on sound measurements or theoretical calculation. It is estimated that the cross section of Penning ionization for most of the metals by argon metastable atoms is of the order of 5×10^{-21} m^2.[22,23] For copper, in particular, a value of 4.87 $\times10^{-21}$ m^2 has been adopted.[24]

The cross section for asymmetric charge transfer is subject to significant uncertainty. The problem has been briefly discussed in Ref. 24 and later on elaborated in Refs. 25 and 26.

The cross sections for all other important collisions taken into consideration are plotted in Fig. 2. The cross section data are taken from Refs. 27–34, respectively.

In addition to the collisions taking place in the plasma, some plasma-surface interactions are also considered. Among them is sputtering caused by Ar^+, Cu^+, and Ar^f. The process is treated according to the semiempirical formula of Matsunami *et al.*[35] that gives the sputtering yield as a function of the energy of the incident particle and the sublimation energy of the cathode material.

Other important interactions on the surface are deexcitation and recombination of the metastable argon atoms and the argon ions, respectively. Both processes are considered complete; i.e., all incident metastables and argon ions are reflected from the wall as argon atoms. The fast argon atoms reaching the walls are also reflected.

In terms of energy, reflection can be elastic or inelastic. In the former, the incident particle is reflected without a change in its velocity magnitude. The postcollision velocity $\boldsymbol{c}$ in this case is given in terms of the precollision speed $c=|\boldsymbol{c}|$

$$c_z=\sqrt{1-U_1},\quad c_x=c\sqrt{U_1}\sin(2\pi U_2),\quad \text{and}$$
$$c_y=c\sqrt{U_1}\cos(2\pi U_2). \tag{7}$$

Here, U_1 and U_2 are independent—homogeneously distributed random numbers in the interval (0,1)—c_z is the velocity component normal to the wall, and c_x and c_y are the velocity components parallel to the wall. Equation (7) represents the cosine distribution law.

The inelastic reflection is also known as thermal accommodation. In this case, the incident particle thermalizes during the collision. When reflected, its energy is equal to the energy that corresponds to the temperature of the wall. If T_w is the wall temperature the postcollision velocity is[36]

$$c_z=\sqrt{\frac{-2k_BT_w\ln U_1}{M}},\quad c_x=c_r\cos\varphi,\quad c_y=c_r\sin\varphi,$$
$$c_r=\sqrt{\frac{-2k_BT_w\ln U_2}{M}},\quad \text{and}\quad \varphi=2\pi U_3. \tag{8}$$

Here, M is the mass of the incident particle while U_1, U_2, and U_3 are independent random numbers.

Which of the two mechanisms that takes place is determined by a parameter called thermal accommodation coefficient. The thermal accommodation coefficient is subject to considerable uncertainty. There are no sufficient data in the literature. At the same time, its value influences the calculation of the gas temperature.[8]

The coefficient of thermal accommodation α is defined as[7]

$$\alpha=\frac{E_{\text{inc}}-E_{\text{refl}}}{E_{\text{inc}}-E_{\text{wall}}},$$

where E_{inc} is the mean energy of the incident particles (the averaging is made after the incident energy has been reduced with the energy of the sputtered particle and the sputtering threshold energy, providing sputtering has taken place), E_{refl} is the mean energy of the reflected particles, and $E_{\text{wall}}(=2k_bT_{\text{wall}})$ is the mean energy of the particles leaving the wall after thermal accommodation. The thermal accommodation coefficient has been assumed equal to 0.5. Therefore, the results are influenced by that choice. The choice has been made based on the following arguments. There are reported values of α of 0.6 for incident energies of 10 eV and $\alpha>0.8$ for incident energies higher than 200 eV for Ar^+ ions on Au and Pt surfaces.[37] At low energies, α drops to 0.2 for the same materials. At the same time, thermal accommodation values have been found to be very similar for different metal surfaces.[38] A parametric study on the influence of the value of α on the calculated amount of gas heating in analytical glow discharges[8] has shown that the results are only slightly changed when varying α between 0.5 and 1.

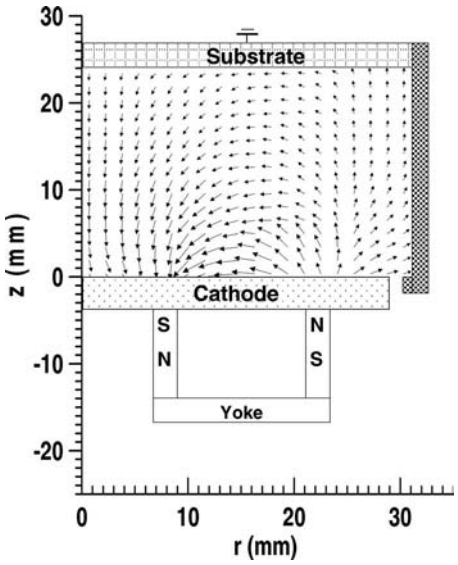

FIG. 3. Scheme of the simulated magnetron discharge. The magnetron is symmetrical relative to the axis $r=0$.

C. Initial condition and operating conditions

The simulation procedure shown in Fig. 1 is applied to the magnetron discharge presented in Fig. 3. The maximum radial magnetic field above the cathode reaches 1300 G. Simulations for pressures of 1, 4, 10, 25, 50, and 100 mTorr are performed. To verify the expected pressure dependence of the gas heating, the parameters of the external circuit have been readjusted in the course of the runs in order to maintain a regime close to constant power. In this way, the power has been 70 $\mathrm{W}\pm 2\%$.

The maximum number of superparticles per type is 900 000. Initially, only electrons and argon ions are assumed with a homogeneous and equal density of 1×10^{14} m^{-3}. The computational grid has 301 nodes in z-direction and 129 nodes in r-direction. The time step is set to 3×10^{-10} s initially and is shortened subsequently to obey the stability criterion. The number of electronic subcycles per ionic cycle is 40. The simulation is run until convergence is obtained in terms of discharge current and particles' densities. This is illustrated in Fig. 4, where the time evolution of the discharge (plasma) and external currents is shown.

To ensure the convergence of the temperature distribution, the maximum gas temperature is traced in time as shown in Fig. 5. It is clear that the relaxation of the maximum temperature occurs at approximately 2 ms. This is about five times earlier than the estimate of 10^{-2} s made in the previous section. The difference is less than an order of magnitude, and it should be mentioned that the estimate has been made for total thermal equilibrium, whereas Fig. 5 presents only the value of the maximum temperature and not the spatial distribution of the temperature. Therefore, it can be concluded that Fig. 5 is satisfactory for the purpose of checking for convergence. Note the different time scales in Figs. 4 and 5. This is in connection to Eq. (2) above.

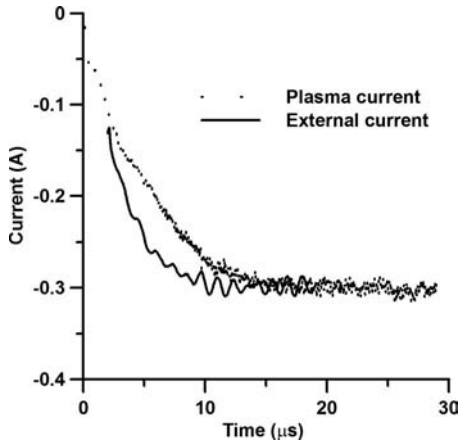

FIG. 4. Time evolution of the calculated plasma (dotted line) and the external (solid line) currents for the case of $p=10$ mTorr. Steady state occurs at time $\mathbf{t}\approx 15$ μs when both currents equalize to a value of approximately 300 mA.

III. RESULTS AND DISCUSSION

A. Temperature distribution

Following the procedure from Fig. 1, the temperature distribution of the gas has been obtained for the five different pressures. At 1 mTorr, there is practically no heating of the gas. The rise of the gas temperature is about 1 K, which is within the limit of the expected error. With the increase in the pressure, the gas begins to heat up. For $p=10$ mTorr, the temperature increases to 316 K, which is about 5% as can be seen in Fig. 6(a). With the increase in the pressure, holding the input electrical power constant, the temperature strongly increases further, being about 600 K at 50 mTorr and reaching to almost 1000 K at 100 mTorr [see Figs. 6(b) and 6(c), respectively]. The increase in the maximum gas temperature with pressure is also illustrated in Fig. 7.

The presented results show that the gas heating is strongly pressure dependent. For the given operating conditions (i.e., feeding gas argon, copper cathode, and input power of 70 W), the gas heating is not significant for pressures of up to 10 mTorr. These are typical conditions for laboratory magnetrons. Commercial sputtering magnetrons

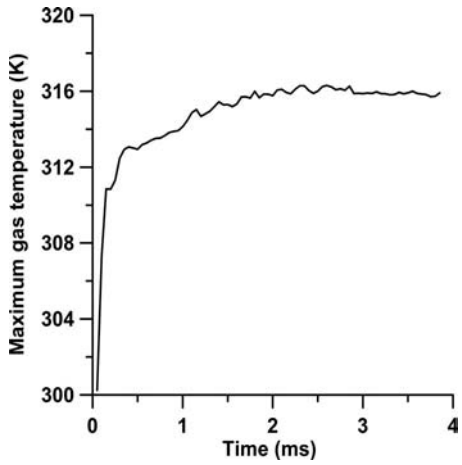

FIG. 5. Relaxation of the maximum gas temperature with time for the case of $p=10$ mTorr.

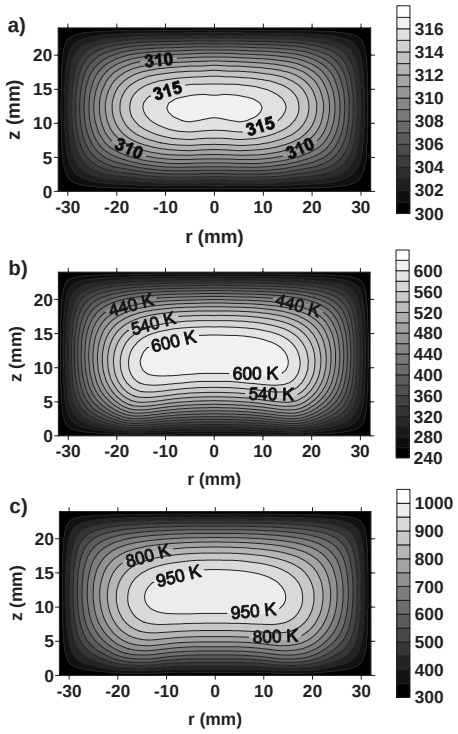

FIG. 6. Contour plot of the calculated gas temperature distribution for the case of (a) $p=10$ mTorr, (b) $p=50$ mTorr, and (c) $p=100$ mTorr.

may be up to ten times bigger and with power supplies of several kilowatts. These operating conditions, however, are outside the scope of this study.

It is interesting to compare the obtained results with other data from the literature. The results for $p=50$ mTorr can be compared to Ref. 7 where the gas heating in a sputtering glow discharge is calculated for $p=42$ mTorr and 40 mm electrode separation. The temperature profile obtained there for a copper electrode and three times higher cathode voltage agrees very well with the gas temperature profile calculated in the present study. The lower voltage in the present case can be easily explained with the magnetic trap leading to much higher discharge efficiency and to some extent with the smaller volume of the gas discharge.

Another comparison can be made with Rossnagel.[2] It is the most often cited work in the literature about the gas heating in sputter magnetrons. The author reports a density reduction of about 37% for a pressure of 30 mTorr and a current of 300 mA. This corresponds reasonably well to our calculation results. Indeed, it can be deduced from Fig. 7 that the gas temperature at 30 mTorr would be around 440 K, which is about 47% higher than 300 K.

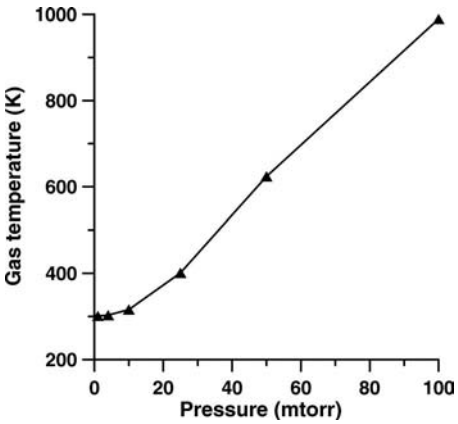

FIG. 7. Calculated maximum gas temperature as a function of the gas pressure at constant electric power. The symbols denote the calculated values.

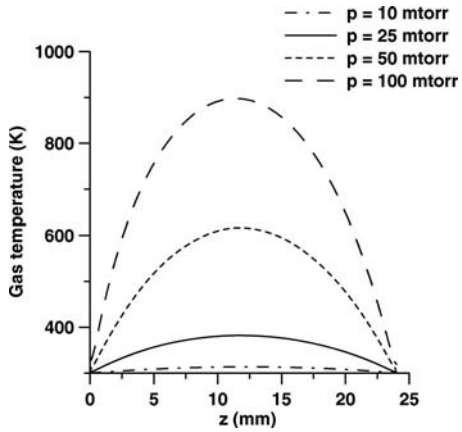

FIG. 8. Calculated gas temperature profile above the racetrack along $r=18.2$ mm for different values of the pressure.

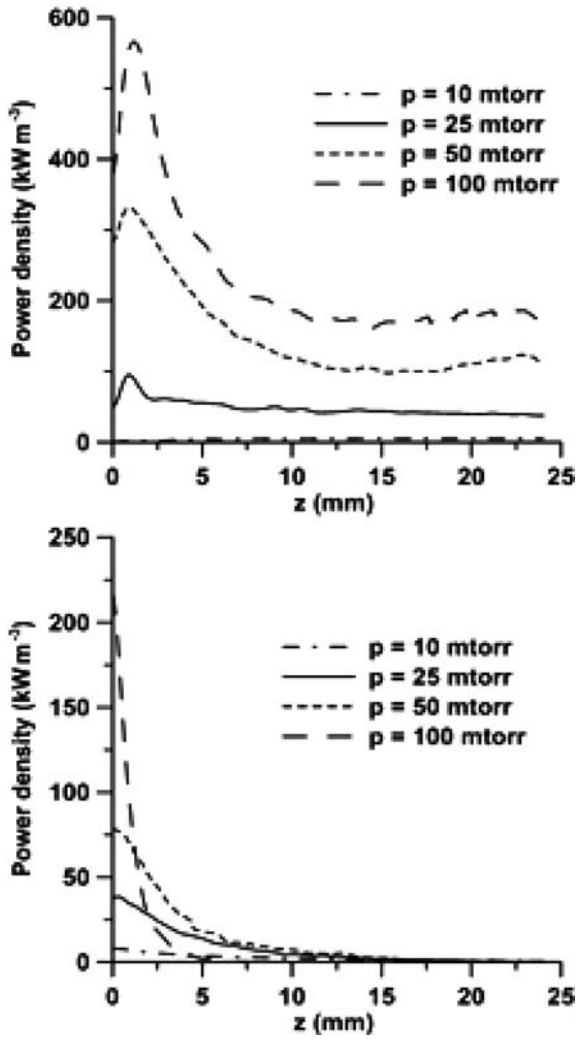

FIG. 9. Calculated axial distribution of the power density deposited in the gas along $r=18.2$ mm for different values of the pressure (a) total and (b) by sputtered copper atoms.

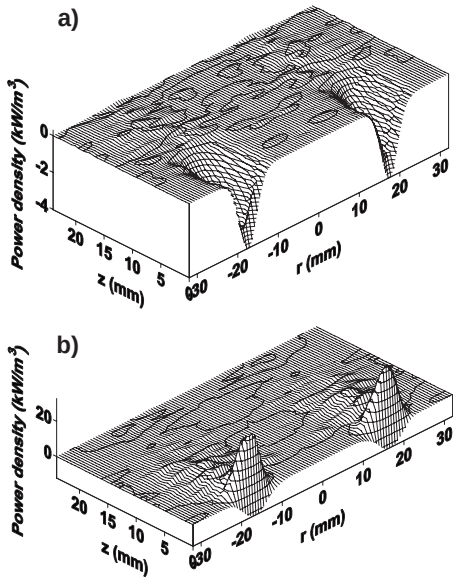

FIG. 10. Calculated distribution of the power density transferred from the ions (Ar^+ and Cu^+) to the gas for the case of (a) $p=10$ mTorr. Note that the value is negative at this low pressure, indicating that the ions mostly create energetic atoms near the cathode, which is counted as cooling of the gas and (b) $p=100$ mTorr. Now the value is mostly positive, indicating that the ions now directly contribute to gas heating in the sheath.

More substantial is the difference with the calculations reported in the recent work of Ekpe and Dew.[3] The maximum temperature there is on average a factor of two higher than the values obtained in our study. In addition, the axial temperature profile is with a different shape. The values of the gas temperature in Ref. 3 are also higher than those in Ref. 2 The shape of the profile in Ref. 3 resembles the shape of those obtained for analytical glow discharges in Ref. 8. The common issue between these two models is that they are entirely or partially fluid. In addition, Ref. 3 is not a self-consistent simulation but is based on several assumptions, each of which brings uncertainties.

The resemblance in the profile shapes (see Fig. 8), the close correspondence of the absolute values of the present work with the kinetic simulation,[7] and the early experimental work[2] indicate that a kinetic self-consistent simulation represents more accurately the considered effect of gas heating in sputter magnetrons at typical operating conditions.

B. Analysis of the power transferred to the gas

Each plasma particle that collides with the gas atoms can transfer power to the gas. Here, the power transfer is counted as positive with respect to the gas if it leads to increase in its temperature. This means that the power transferred to the gas, which results in the creation of energetic (nonthermal) gas atoms is counted as negative because it actually absorbs thermal energy from the gas [see Eq. (3) above]. As it has been mentioned above, this separation is sensitive to the thermal limit [see Eq. (4)], above which the atoms are considered energetic. This formalism leads to the following consequences. A fast heavy particle needs several interactions with the background gas atoms before it can directly contribute to gas heating. This means that during the first several collisions, the result will not be a rise in the gas temperature but the creation of fast gas atoms. These fast atoms subsequently collide with the thermal atoms and contribute directly to the gas heating. This leads to enlargement of the region where the power is transferred effectively to the gas.

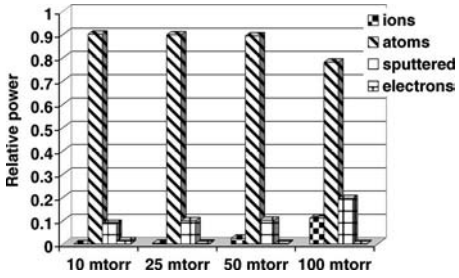

FIG. 11. Calculated relative contribution to the total power transferred to the argon gas (integrated over the whole discharge) for ions, atoms, sputtered atoms, and electrons for different pressures.

The total power input, summed over all contributors, is pressure dependent as can be seen in Fig. 9(a). The power deposition is almost constant with respect to the distance from the cathode at low pressure, whereas with the increase in the pressure, more power is deposited near the cathode. This is explained with the change in the proportion of each type of plasma species to the total power deposition. For example, sputtered atoms thermalize much faster at higher pressure; and therefore, their direct contribution to the total power increases, especially adjacent to the cathode [see Fig. 9(b)]. The same holds for the ions. When they accelerate in the sheath at low pressure, they mostly create energetic neutrals, which are counted as cooling of the gas, hence a negative power deposition [see Fig. 10(a)]. For the time of their fall to the cathode, the ions cannot suffer enough collisions to begin to contribute to the deposited power directly. At high pressure, however, more ions can directly contribute to the gas heating, as shown in Fig. 10(b).

The power, integrated over the whole discharge, deposited by the different plasma species as a function of the pressure is presented in Fig. 11. It is clear that for all pressures the collisions between argon atoms are the main contributors to the gas heating. This means that ions and sputtered atoms transfer their energy to the thermal gas atoms mostly indirectly. At low pressure, the ions transfer more energy to energetic gas atoms than to the thermal gas atoms. That is why their relative contribution to the heating is even lower than that of electrons, even though the mass of the latter is so much smaller. This result shows the necessity of the inclusion of the fast neutrals in models when the gas heating should be accounted for.

IV. CONCLUSION

The present work has investigated the effect of gas heating in laboratory sputter magnetrons by means of kinetic numerical simulations. The proposed model describes all relevant processes in the magnetron chamber in a completely self-consistent way. Its distinctive advantage is the ability to simultaneously simulate processes with large difference in their characteristic times (several orders of magnitude). The results of the model indicate that gas heating takes place and should be taken into consideration at pressures above several

milliTorr at typical operating power. The gas temperature rises distinctively when the pressure increases. At pressure range between 1 and 10 mTorr, gas heating can be disregarded in models and estimates. The charged heavy particles (gas and sputtered ions) cannot thermalize and transfer the energy of the applied electric field to the thermal gas background by creating fast gas neutrals. This suggests that for a correct description of magnetrons fast gas atoms should be included in the analysis.

The results of the model are in good correspondence with the available experimental data.[2] The calculated gas temperature is approximately two times lower than the temperature calculated with a non-self-consistent fluid model for similar operating conditions.[3] The better agreement of our data with the experimental measurements manifests the need for kinetic self-consistent modeling of sputter magnetrons.

ACKNOWLEDGMENTS

The authors are grateful to Professor Renaat Gijbels for the useful discussions and valuable advises.

This work has been financially supported through the project "New Research Initiative" of the University of Antwerp. Calculations were performed on the CALCUA supercomputer of the University of Antwerp.

[1] D. F. Hoffman, J. Vac. Sci. Technol. A **3**, 561 (1985).
[2] S. M. Rossnagel, J. Vac. Sci. Technol. A **6**, 19 (1988).
[3] S. D. Ekpe and S. K. Dew, J. Phys. D **39**, 1413 (2006).
[4] R. S. Robinson, J. Vac. Sci. Technol. **16**, 185 (1979).
[5] G. M. Turner, J. Vac. Sci. Technol. A **13**, 2161 (1995).
[6] A. Palmero, H. Rudolph, and F. H. P. M. Habraken, Appl. Phys. Lett. **87**, 071501 (2005).
[7] V. Serikov and K. Nanbu, J. Appl. Phys. **82**, 5948 (1997).
[8] A. Bogaerts, R. Gijbels, and V. Serikov, J. Appl. Phys. **87**, 8334 (2000).
[9] I. Revel, L. C. Pitchford, and J. P. Boeuf, J. Appl. Phys. **88**, 2234 (2000).
[10] I. Kolev and A. Bogaerts, Contrib. Plasma Phys. **44**, 582 (2004).
[11] I. Kolev and A. Bogaerts, IEEE Trans. Plasma Sci. **34**, 886 (2006).
[12] I. Kolev, A. Bogaerts, and R. Gijbels, Phys. Rev. E **72**, 056402 (2005).
[13] I. Kolev, Ph.D. thesis, University of Antwerp, 2007.
[14] E. Bultinck, I. Kolev, A. Bogaerts, and D. Depla, J. Appl. Phys. **103**, 013309 (2008).
[15] I. P. Bazarov, *Thermodynamics* (Pergamon, New York, 1964).
[16] R. L. Powell and G. E. Childs, in *American Institute of Physics Handbook*, edited by D. E. Grey (McGraw-Hill, New York, 1972).
[17] Y. P. Raizer, *Gas Discharge Physics* (Nauka, Moscow, 1987).
[18] C. K. Birdsall and A. B. Langdon, *Plasma Physics via Computer Simulations* (Hilger, Bristol, 1991).
[19] V. Serikov and K. Nanbu, J. Vac. Sci. Technol. A **14**, 3108 (1996).
[20] J. O. Hirschfelder, C. F. Curtiss, and R. B. Bird, *Molecular Theory of Gases and Liquids* (Wiley, New York, 1964).
[21] P. N. Swartztrauber, SIAM (Soc. Ind. Appl. Math.) J. Numer. Anal. **11**, 1136 (1974).
[22] L. A. Riseberg, W. F. Parks, and L. D. Schearer, Phys. Rev. A **8**, 1962 (1973).
[23] M. Bourène and J. Le Calve, J. Chem. Phys. **58**, 1452 (1973).
[24] A. Bogaerts, J. Appl. Phys. **79**, 1279 (1996).
[25] A. Bogaerts and R. Gijbels, J. Anal. At. Spectrom. **11**, 841 (1996).
[26] A. Bogaerts, K. A. Temelkov, N. K. Vuchkov, and R. Gijbels, Spectrochim. Acta, Part B **62**, 325 (2007).
[27] N. J. Mason, J. Phys. B **20**, 1357 (1987).
[28] H. A. Hyman, Phys. Rev. A **18**, 441 (1978).
[29] H. A. Hyman, Phys. Rev. A **20**, 855 (1979).
[30] L. Vriens, Phys. Lett. **8**, 260 (1964).
[31] A. V. Phelps and B. M. Jelenkovic, Phys. Rev. A **38**, 2975 (1988).
[32] J. Lindhard, M. Scharff, and H. E. Schiott, Mat. Fys. Medd. K. Dan. Vidensk. Selsk. **33**, 3 (1963).
[33] A. V. Phelps, C. H. Greene, and J. P. Burke, Jr., J. Phys. B **33**, 2965 (2000).
[34] A. V. Phelps, J. Phys. Chem. Ref. Data **20**, 557 (1991).
[35] N. Matsunami, Y. Yamamura, Y. Itikawa, N. Itoh, Y. Kazumata, S. Miyagava, K. Morita, R. Shimizu, and H. Tawara, At. Data Nucl. Data Tables **31**, 1 (1984).
[36] V. Serikov and K. Nanbu, Rep. Inst. Fluid Sci. **6**, 43 (1994).
[37] H. F. Winters, H. Coufal, C. T. Rettner, and D. S. Bethune, Phys. Rev. B **41**, 6240 (1990).
[38] H. Coufal, H. F. Winters, H. L. Bay, and W. Eckstein, Phys. Rev. B **44**, 4747 (1991).